

7D-folding integral in a density-dependent microscopic optical model potential for nucleon-nucleus scattering

H. F. Arellano^{1,2,*} and E. Bauge^{2,†}¹*Department of Physics-FCFM, University of Chile, Av. Blanco Encalada 2008, Santiago, Chile*²*CEA/DAM/DIF, F-91297 Arpajon, France*

(Received 19 May 2011; published 14 September 2011)

Microscopic optical model potentials, based on density-dependent effective interactions, involve multidimensional integrals to account for the full Fermi motion of the target struck nucleon throughout the nucleus. If a spherical matter distribution is assumed, then each matrix element of the optical potential requires the evaluation of seven-dimensional integrals. In this work we provide a full account of these integrals, retaining the genuine off-shell structure of the nucleon-nucleon effective interaction. The evaluation is based on the asymptotic separation of the optical model potential for nucleon-nucleus scattering in momentum space, where the potential is split into a free t -matrix contribution and another which depends exclusively on the gradient of the density-dependent g matrix. The calculated potentials, based on the Paris nucleon-nucleon (NN) potential, are applied to proton elastic scattering from ^{16}O and ^{90}Zr at beam energies between 30 and 65 MeV. The results were compared with two approximations to the unabridged expression, revealing moderate differences among their scattering observables. When comparing with results based on the Argonne v_{18} NN potential, these differences appear smaller than those attainable by the choice of the internucleon potential.

DOI: [10.1103/PhysRevC.84.034606](https://doi.org/10.1103/PhysRevC.84.034606)

PACS number(s): 24.10.Ht, 21.60.-n, 25.60.Bx, 25.40.Cm

I. INTRODUCTION

The optical model potential constitutes an essential tool for investigating nuclear collisions and reactions. Its use provides not only a direct account for scattering observables but also quantitative information about the distortion of the scattered waves, a very useful input for the study of inelastic processes. In the particular case of folding models for nucleon-nucleus (NA) scattering, the optical model potential becomes a one-body operator relying on a fundamental link between the medium-free nucleon-nucleon (NN) interaction and an effective interaction which embodies, in principle, all correlations implicit in a $(A + 1)$ -nucleon system [1–7]. However, the complexity of the problem is such that this link becomes feasible only with the introduction of simplifying assumption. These simplifications come not only after truncations in the perturbative expansions for the effective interaction but also from the treatment of its coordinate- and/or momentum-space structure. In this work we focus on the latter issue, providing a complete account of the Fermi motion of the struck nucleon while retaining the exact momentum structure of the genuine effective interaction, as obtained from the Brueckner-Bethe-Goldstone for infinite nuclear matter. This feature contrasts with all previous density-dependent approaches [7–11], where simplifications are introduced at the level of the effective interaction (localization) or its momentum dependence.

The study we present here is based on a recent finding indicating that intrinsic nuclear medium effects, namely those arising from the density dependence of the g matrix, are dominantly localized on the nuclear surface, i.e., regions where the gradient of g is strongest [12]. The result is

an analytic consequence of the momentum- and coordinate-space structure of a two-body effective interaction spherically symmetric in the mean coordinate of the interacting pair. Quite generally, any two-body interaction can be expressed as a nontrivial sum of a translationally invariant term and another which is functionally—and exclusively—proportional to the gradient of a reduced *in-medium* interaction. As a result, the *unabridged* optical potential in momentum space becomes the sum of medium-free (free t matrix) and medium-dependent (g matrix) contributions, the latter depending exclusively on the variations of the effective interaction with respect to the mean coordinate. The term unabridged has been coined here to stress the fact that the full momentum structure, as dictated by the exact kinematics of the colliding nucleons, is retained throughout.

A simplified version of the unabridged potential was investigated in Ref. [11] within the framework of so-called δg -folding. There the momentum dependence of the effective interaction on the struck-nucleon recoil was treated approximately, by evaluating the relative momenta as if the two-nucleon interaction conserves total momentum. This simplification was referred to as a momentum-conserving approximation, a feature which would emerge only if the interaction was translationally invariant.

Current trends in nuclear research and applications have resulted in the development and construction of novel research facilities aimed at studying exotic nuclei. Such is the case of radioactive ion beam accelerators in the United States, Europe, and Japan [13–18], where intense rare isotope beams are produced and collided against selected targets. When these beams are scattered from hydrogen targets, the process reduces to the traditional NA collision. For instance, if the ion beam reaches an energy of $60A$ MeV, the collision would be equivalent to that of a 60-MeV proton scattering from the nucleus of the ion. This equivalence in the center-of-mass

* arellano@dfi.uchile.cl

† eric.bauge@cea.fr

reference frame leads us—for ion beams below 100A MeV—to revisit an energy regime where the inclusion of medium effects is known to be critical. Hence, from the NA scattering point of view, counting on accurate approaches capable of tracking selectively the various contributions to the optical model potential—particularly its surface structure—becomes essential for studying and interpreting data from rare-isotope beam facilities. Along this line, an assessment of the implications of alternative simplifications of the unabridged optical potential, based on the actual evaluation of this operator, is quite relevant if one needs to incorporate high-order effects to describe the data.

This paper is organized as follows. In Sec. II we outline the general framework, discuss the structure of the unabridged optical model potential, introduce the δg -folding approach, and make contact with known approximations. Additionally, we examine more closely the various contributions to the optical potential. In Sec. III we present and discuss results from selected applications of proton elastic scattering at energies between 30 and 65 MeV. In Sec. IV we summarize this work and present the main conclusions.

II. THEORETICAL FRAMEWORK

From a broad perspective, diverse formal expressions of the optical model potential for NA scattering can be found in the literature [1–5]. Although they may differ in the way contact is made with the bare NN interaction, they all take the form of a ground-state expectation value of a generalized two-body interaction. Thus, a general representation of the optical model potential for collisions of nucleons with kinetic energy E off a composite A -nucleon target can be expressed as

$$U(\mathbf{k}', \mathbf{k}; E) = \int d\mathbf{p}' d\mathbf{p} \langle \mathbf{k}' \mathbf{p}' | \hat{T}(E) | \mathbf{k} \mathbf{p} \rangle_{\mathcal{A}} \hat{\rho}(\mathbf{p}', \mathbf{p}), \quad (1)$$

where the subscript \mathcal{A} stands for antisymmetrization. Isospin labels are omitted to simplify notation. In general, \hat{T} contains information about the discrete spectrum of the many-body system. In this expression $\hat{\rho}(\mathbf{p}', \mathbf{p})$ represents the one-body (off-shell) mixed density corresponding to the ground state of the target,

$$\hat{\rho}(\mathbf{p}', \mathbf{p}) = \sum_{\alpha} \langle \alpha | \mathbf{p}' \rangle \langle \mathbf{p} | \alpha \rangle. \quad (2)$$

Here α denotes occupied single-particle states of the target.

A comprehensive evaluation of the optical potential considering the full \hat{T} matrix would require the solution of the $(A+1)$ -body system, a challenge which goes beyond our current capabilities. This difficulty can be circumvented by decoupling the two-body effective interaction from the ground-state structure, a suitable strategy at intermediate and high energies when the discrete spectrum of the many-body Green's function is away from the projectile energy in the continuum. This allows the use of single-particle models to describe the target ground state and the Brueckner-Bethe-Goldstone reaction matrix to represent the effective interaction.

As expressed in Eq. (1), a central element in the evaluation of the optical potential is the representation of the

two-body effective interaction. Quite generally, regardless of the physics content or particular structure conceived for the NN interaction, the two-body operator \hat{T} in coordinate space requires the specification of four vectors. This leads to matrix elements of the form $\langle \mathbf{r}' \mathbf{s}' | \hat{T} | \mathbf{r} \mathbf{s} \rangle$, where \mathbf{r} and \mathbf{s} denote the “prior” coordinates of the projectile and target nucleon, respectively. The primed vectors refer to “post” coordinates. With these definitions, the *mean coordinate* \mathbf{z} becomes

$$\mathbf{z} = \frac{1}{4}(\mathbf{r}' + \mathbf{r} + \mathbf{s}' + \mathbf{s}),$$

corresponding to the mean coordinate among the prior and post coordinates of the interacting particles.

As demonstrated in Ref. [12], the momentum-space representation of the \hat{T} matrix can be cast in terms of a reduced interaction, g_z , in the form

$$\langle \mathbf{k}' \mathbf{p}' | \hat{T} | \mathbf{k} \mathbf{p} \rangle = \int \frac{d\mathbf{z}}{(2\pi)^3} e^{i\mathbf{z} \cdot (\mathbf{Q} - \mathbf{q})} g_z(\mathbf{K}_{\parallel}; \mathbf{b}', \mathbf{b}). \quad (3)$$

Here we denote

$$\mathbf{q} = \mathbf{k} - \mathbf{k}', \quad \mathbf{Q} = \mathbf{p}' - \mathbf{p}, \quad (4)$$

accounting for the momentum transfer of the projectile and recoil of the target nucleon, respectively. Additionally,

$$\mathbf{K} = \frac{1}{2}(\mathbf{k} + \mathbf{k}'), \quad \mathbf{P} = \frac{1}{2}(\mathbf{p}' + \mathbf{p}) \quad (5)$$

represent the mean momentum of the projectile and struck nucleon, respectively. In terms of these momenta, the post and prior relative momenta can be expressed as

$$\mathbf{b}' = \frac{1}{2}(\mathbf{k}' - \mathbf{p}') = \frac{1}{2}[\mathbf{K} - \mathbf{P} - \frac{1}{2}(\mathbf{q} + \mathbf{Q})], \quad (6a)$$

$$\mathbf{b} = \frac{1}{2}(\mathbf{k} - \mathbf{p}) = \frac{1}{2}[\mathbf{K} - \mathbf{P} + \frac{1}{2}(\mathbf{q} + \mathbf{Q})], \quad (6b)$$

respectively. In Eq. (3)

$$\mathbf{K}_{\parallel} = \mathbf{K} + \mathbf{P} \quad (7)$$

can be interpreted as the current of the interacting nucleons, consisting of the sum of the prior and post mean momenta of the colliding pair. With these definitions the integrals over $(\mathbf{p}, \mathbf{p}')$ in Eq. (1) are accounted for by (\mathbf{P}, \mathbf{Q}) , with $d\mathbf{p}' d\mathbf{p} = d\mathbf{Q} d\mathbf{P}$.

What is appealing about the above representation for \hat{T} is that it prescribes naturally, without ad hoc assumptions, the way the medium dependence of the two-body interaction is mapped through the mean coordinate \mathbf{z} in the reduced interaction. In this respect we follow the conventional route [7–9], assuming that this site dependence is driven by the local density, i.e., a local density approximation. Thus, to each site \mathbf{z} in the nucleus we associate the isoscalar local density $\rho(\mathbf{z})$ with its corresponding symmetric nuclear matter Brueckner-Bethe-Goldstone reaction matrix g_z (g matrix) satisfying

$$g(\omega) = v + v \frac{\hat{Q}}{\omega + i\eta - \hat{h}_1 - \hat{h}_2} g(\omega). \quad (8)$$

Here v is the bare NN potential, \hat{h}_1 and \hat{h}_2 are the quasiparticle energies at density ρ , and \hat{Q} is the Pauli blocking operator to

suppress the propagation on occupied intermediate states. The corresponding Fermi momentum is given by

$$k_F = (3\pi^2 \rho)^{1/3}. \quad (9)$$

In a finite system, i.e., a system with a confined matter distribution, we note that $\rho(z) \rightarrow 0$ as $z \rightarrow \infty$. Therefore

$$\lim_{z \rightarrow \infty} g_z(\omega) = t(\omega), \quad (10)$$

the free-space t matrix.

In the context of a spherically symmetric matter distribution [$\rho(z) \rightarrow \rho(z)$], the z integral in Eq. (3) can be split in such a way that its asymptotic structure becomes isolated from the z -dependent term [12]. Accordingly,

$$\begin{aligned} \langle \mathbf{k}' \mathbf{p}' | \hat{T} | \mathbf{k} \mathbf{p} \rangle &= \delta(\mathbf{Q} - \mathbf{q}) t(\mathbf{K}_{\parallel}; \mathbf{b}', \mathbf{b}) \\ &- \frac{1}{6\pi^2} \int_0^{\infty} z^3 dz \mathcal{S}(z|\mathbf{Q} - \mathbf{q}) \frac{\partial g_z}{\partial z}, \end{aligned} \quad (11)$$

where the momentum dependence of $\partial g_z / \partial z$ on \mathbf{K}_{\parallel} , \mathbf{b}' , and \mathbf{b} is implicit. Here $\mathcal{S}(x) = 3j_1(x)/x$, with $j_1(x)$ the spherical Bessel function of order 1. This function peaks at $x = 0$, favoring the recoil of the struck nucleon around $\mathbf{Q} \approx \mathbf{q}$, namely, $\mathbf{k} + \mathbf{p} \approx \mathbf{k}' + \mathbf{p}'$. Notice that total momentum conservation becomes possible only under translational invariance of the system, as expressed when $\partial g_z / \partial z = 0$.

It is worth noting that a critical shortcoming of Eq. (3) for \hat{T} is its weak convergence for the spatial integration under the z coordinate. This is evident by the fact that the reduced interaction g_z does not vanish as $z \rightarrow \infty$. In this respect, the asymptotic separation extracts the momentum-conserving contribution (a δ function), leaving the medium contribution localized in space. This feature becomes crucial in the actual implementation of the unabridged integrals of the optical potential.

Upon substitution of \hat{T} from Eq. (11) into Eq. (1) for the optical potential we obtain for its unabridged form

$$U = U_0 + U_1, \quad (12)$$

with

$$U_0 = \int d\mathbf{P} \hat{\rho}(\mathbf{q}; \mathbf{P}) t(\mathbf{K}_{\parallel}; \mathbf{b}', \mathbf{b}), \quad (13a)$$

$$U_1 = \frac{-1}{6\pi^2} \int_0^{\infty} z^3 dz \int d\mathbf{Q} d\mathbf{P} \hat{\rho}(\mathbf{Q}; \mathbf{P}) \mathcal{S}(z|\mathbf{Q} - \mathbf{q}) \frac{\partial g_z}{\partial z}. \quad (13b)$$

Here we denote

$$\hat{\rho}(\mathbf{Q}; \mathbf{P}) \equiv \hat{\rho}(\mathbf{P} + \frac{1}{2}\mathbf{Q}, \mathbf{P} - \frac{1}{2}\mathbf{Q}).$$

The first term, U_0 , depends exclusively on the reduced matrix in free space. This contribution is referred to as the *full-folding* optical potential, with its first realizations in momentum space reported in the early 1990s [6,19–22]. In this case the effective interaction is taken as the off-shell scattering matrix in the framework of the Lippmann-Schwinger equation. The second term, U_1 , depends on the gradient with respect to the mean coordinate of the g matrix. It involves a seven-fold integral,

one of them along the radial coordinate and the other six to account for the Fermi motion of the struck nucleon [11].

We have been able to evaluate the unabridged optical potential as expressed by Eqs. (12), (13a), and (13b). In this paper we report applications for proton elastic scattering and compare their corresponding observables with those from two approximations in hierarchical order. One of them is the so-called δg -folding [11], where the \mathbf{Q} dependence of \mathbf{b} and \mathbf{b}' in the gradient $\partial g_z / \partial z$ is neglected, by setting $\mathbf{Q} \rightarrow \mathbf{q}$. This enables us to isolate the evaluation of the $d\mathbf{Q}$ integral in Eq. (13b),

$$\int d\mathbf{Q} \hat{\rho}(\mathbf{Q}; \mathbf{P}) \mathcal{S}(z|\mathbf{Q} - \mathbf{q}),$$

involving only the mixed density and the \mathcal{S} function. With this small change the reckoning time for the δg -folding becomes shorter, by nearly a factor 25, than the one needed for the unabridged evaluation. Still, both approaches are general enough to treat explicitly the off-shell mixed density of the target.

From a physical standpoint, under the δg -folding scheme the recoil of the struck nucleon is treated as if the total momentum of the interacting pair was conserved. The extent to which this consideration is reliable would depend on the off-shell behavior of the medium-dependent effective interaction. As noted previously, since medium effects appear in the form of a gradient of the effective interaction, any manifestation of these effects would stem from the surface of the nucleus.

The next level of approximation departs from the δg -folding, approximating the mixed density according to the Slater prescription [23]. In this case

$$\begin{aligned} \hat{\rho}(\mathbf{Q}; \mathbf{P}) &\approx \hat{\rho}_{\text{SL}}(\mathbf{Q}; \mathbf{P}) \\ &= 4\pi \int_0^{\infty} z^2 dz j_0(Qz) \rho(z) \frac{3}{4\pi \hat{k}_z^3} \Theta(\hat{k}_z - P), \end{aligned}$$

where the local momentum \hat{k}_z is dictated by the local density at coordinate z through $\hat{k}_z = [3\pi^2 \rho(z)]^{1/3}$. With this prescription for $\hat{\rho}$, the δg -folding optical potential takes the form of the *in-medium* folding model introduced by Arellano, Brieva, and Love (ABL) [10]. More explicitly,

$$U = 4\pi \int_0^{\infty} z^2 dz j_0(qz) \rho(z) \bar{g}_z, \quad (14)$$

with \bar{g}_z an off-shell average of the g matrix given by

$$\bar{g}_z = \frac{3}{4\pi \hat{k}_z^3} \int d\mathbf{P} \Theta(\hat{k}_z - |\mathbf{P}|) g_z(\mathbf{K}_{\parallel}; \mathbf{b}^-, \mathbf{b}^+),$$

where $\mathbf{b}^{\pm} = \frac{1}{2}(\mathbf{K} - \mathbf{P} \pm \mathbf{q})$. Here again a significant reduction in the computing time is achieved, making the ABL approach nearly 20 times briefer than that for the δg -folding.

An appealing feature of the Slater approximation is that its form factor is coincident with the one obtained for the local density $\rho(z)$ or shell-model wave functions, i.e.,

$$\bar{\rho}(q) = \int \hat{\rho}(\mathbf{Q}; \mathbf{P}) d\mathbf{P} = \int \hat{\rho}_{\text{SL}}(\mathbf{Q}; \mathbf{P}) d\mathbf{P}.$$

Therefore, a contrast between the δg - and ABL-folding calculations serves to gauge the way the effective interaction

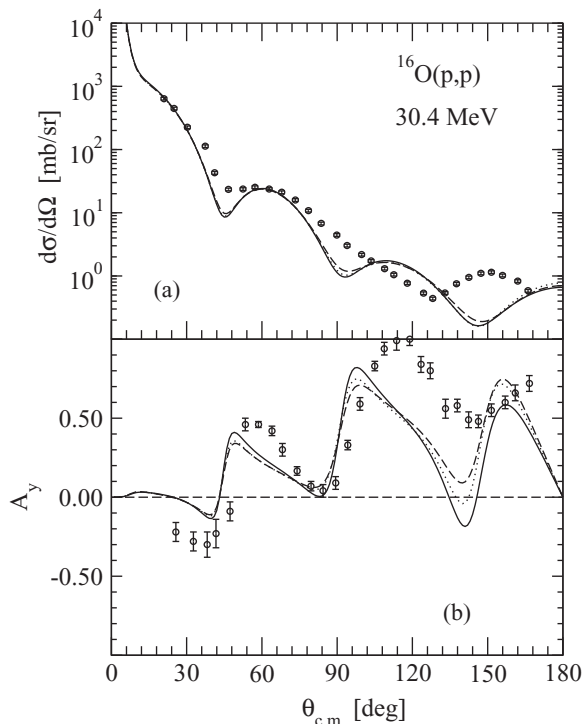


FIG. 1. Measured [29] and calculated differential cross section (a) and analyzing power (b), as functions of the center-of-mass scattering angle, for $^{16}\text{O}(p,p)$ scattering at 30.4 MeV. The solid, dashed, and dotted curves represent the unbridged, δg -folding, and ABL-folding results, respectively.

is weighed off shell—within this constraint—when the Fermi motion under the \mathbf{P} integral is accounted for.

The three forms of the optical potential just discussed yield nonlocal operators, functions of the beam energy E , which in momentum space depend on two momenta and their relative angle, i.e., $U(\mathbf{k}', \mathbf{k}; E)$. The nonlocality is a consequence of the momentum-space structure of the g matrix, solutions of the Brueckner-Bethe-Goldstone integral equation. We stress here that no parametrization nor localization procedures are used to represent these solutions. The antisymmetrization of the interaction accounts for additional nonlocalities.

III. APPLICATIONS

In this section we present results from applications based on the three approaches for the optical potential described above. These are, in decreasing hierarchy, the unbridged, the δg -folding, and the ABL-folding models. We focus on proton elastic scattering from ^{16}O and ^{90}Zr , two relatively well known doubly-closed-shell nuclei. The one-body mixed density is constructed using single-particle wave functions based on Hartree-Fock calculations [24].

The microscopic calculations reported here are based on the Paris NN potential [25]. The corresponding g matrix was calculated off shell ($J \leq 7$) at 15 values for the Fermi momentum, ranging from 0 to 1.5 fm^{-1} . The starting energy is given by the NA kinetic energy at the center of mass, plus the single-particle average binding at the corresponding density

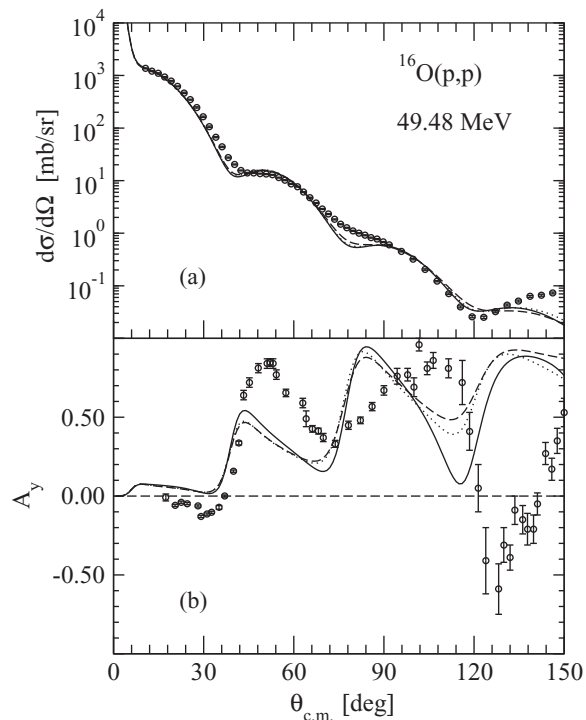


FIG. 2. The same as Fig. 1 but at 49.48 MeV. The data are from Ref. [30].

[26]. For simplicity, the calculations reported here take the Fermi average of K_{\parallel} , with $|\mathbf{K}| = k_{\circ}$, the on-shell momentum in the NA center of mass. Only under this consideration does the evaluation of the unbridged potential become feasible. Otherwise we would need to take into account contributions due to bound pn pairs in nuclear matter, as discussed in Ref. [27].

The self-consistent nuclear-matter fields were computed prior to all runs following conventional approaches in the treatment of the particle-particle propagator, i.e., angle-averaged Pauli blocking and angle-averaged energy denominator. Since our aim here is to provide a consistent comparison among all three approaches, we have chosen to leave for future studies other issues such as alternative treatments in the calculation of the Brueckner-Bethe-Goldstone g matrix [36], the inclusion of higher order effects, or exploration of nonconventional effects such as three-body forces.

To evaluate U_1 given by Eq. (13b) we carry out the \mathbf{P} and \mathbf{Q} integrals using Gauss-Laguerre quadratures. We carried out several tests of convergence, making sure that the numerical quadratures were adequate enough to fulfill equivalences under certain limit cases. The z integration is performed using a uniform mesh with steps of 0.1 fm. The matrix elements $U(\mathbf{k}', \mathbf{k}; E)$ are calculated at 34 momenta in the range $[0, 10 \text{ fm}^{-1}]$. The angular mesh follows a Gaussian setting with as many knots as partial waves needed for convergence in the scattering calculations. This feature makes the unbridged calculations severely intensive for large targets at energies above 100 MeV, an important consideration to leave them unattended in this study. The actual CPU time to evaluate the unbridged potentials reported here ranges from 400 h,

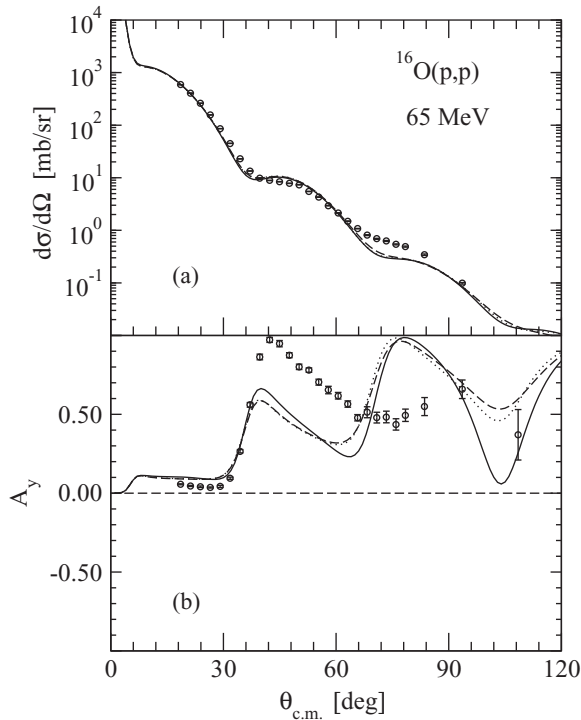


FIG. 3. The same as Fig. 1 but at 49.48 MeV. The data are from Ref. [31].

in the case of $^{16}\text{O}(p,p)$ at 30 MeV, to 700 h in the case of $^{90}\text{Zr}(p,p)$ at 65 MeV. This is using a standard 2.5-Gz processor. The real execution time is significantly reduced with the use of multiprocessor platforms. The scattering observables were calculated by solving the Schrödinger equation with a nonlocal coupling in the presence of the Coulomb potential [28].

A. Scattering applications

In Figs. 1, 2, and 3 we show the measured and calculated observables for $^{16}\text{O}(p,p)$ at 30.4, 49.48, and 65 MeV, respectively. Here the differential cross section $d\sigma/d\Omega$ (a) and analyzing power A_y (b) are plotted as functions of the center-of-mass scattering angle $\theta_{c.m.}$. The data at each of these energies are from Refs. [29], [30], and [31], respectively. Solid, dashed, and dotted curves represent the unbridged, δg -folding, and ABL-folding results, respectively.

At 30.4 MeV shown in Fig. 1 we observe that the cross section is rather poorly described by the three approaches. For instance, the shallow first minimum in the measured $d\sigma/d\Omega$ gets overestimated by the theory, while near 90° and 150° the calculated cross sections exhibit nonexistent minima. In the case of the analyzing power, even though the calculated peaks become comparable to the data, they appear shifted to forward angles relative to the measured values.

In the cases of 40.48 and 65 MeV shown in Figs. 2 and 3, the agreement between the calculated and measured cross sections improves considerably, with slight disagreements near the shoulders exhibited by the data. However, the calculated first peak of the analyzing powers are weaker by nearly 40%

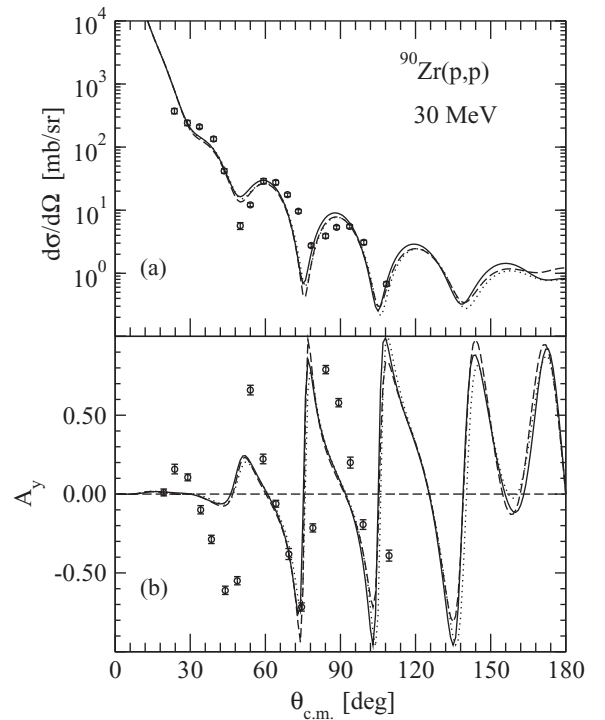


FIG. 4. Measured [32] and calculated differential cross section (a) and analyzing power (b), as functions of the center-of-mass scattering angle, for $^{90}\text{Zr}(p,p)$ scattering at 30 MeV. The solid, dashed, and dotted curves represent the unbridged, δg -folding, and ABL-folding results, respectively.

relative to the data. Not only that, but also the calculated A_y appears shifted to forward angles with respect to the data.

When comparing the three approaches at these energies we note that they are quite similar to each other, with more visible differences in the case of A_y at large scattering angles. This finding is quite interesting since it validates the use of the δg - and ABL-folding approaches to represent the unbridged folding model. Apart from the computing time, the advantage of the ABL approach lies in its versatility, whereas for the δg -folding relies on its ability to provide an explicit treatment to shell-model wave functions.

The cases for $^{90}\text{Zr}(p,p)$ scattering are shown in Figs. 4, 5, and 6. Here we plot the measured and calculated differential cross section (a) and analyzing power (b), as functions of the center-of-mass scattering angle, for proton energies of 30, 40, and 65 MeV, respectively. Their respective data are from Refs. [32], [33], and [31]. Here we observe an even closer similarity in the calculated observables among all three approaches. Once again, differences among these schemes appear more visible in the analyzing power.

B. Paris versus Argonne v_{18} potentials

In order to gauge the significance in the dispersion due to the three approaches considered above, all of them based on the Paris NN potential, we have calculated optical potentials in the ABL approach using the Argonne v_{18} NN potential [34]. These two realistic NN models constitute reasonable

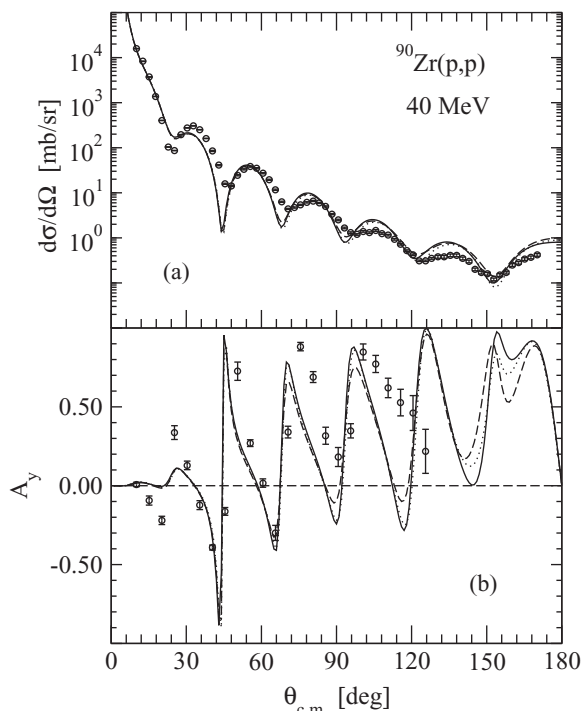


FIG. 5. The same as Fig. 4 but at 40 MeV. The data are from Ref. [33].

representatives of the most complete current descriptions of the basic interaction. Although they are not identical in the description of the NN data, i.e., the on-shell g matrix at zero density, they become useful for assessing the level of uncertainty attainable to the representation of the bare two-body potential.

In the upper frames (a) of Figs. 7 and 8 we present the differential cross section based on the Paris (curves with error bars) and the Argonne v_{18} (dashed curves) NN potential models, as functions of $\theta_{c.m.}$. The red curves represent the average among the unabridged, δg -folding, and ABL-folding results, whereas the error bars extend from their lowest to highest value at a given angle. An identical procedure is followed for the analyzing powers (b).

It is interesting to note that, overall, the calculated observables based on the v_{18} interaction can be discriminated from the bars defined for the Paris potential. This means that the uncertainties implied by the choice of a given approach to evaluate the optical potential are smaller than those attainable by the choice of a realistic NN model. As mentioned before, these differences are a manifestation of on- and off-shell effects at zero density and the way they manifest themselves in the nuclear medium.

To complement these comparisons, in Table I we summarize the resulting reaction cross section (σ_R) from all applications discussed previously. In the sixth column we show the results based on the ABL approach using the AV18 potential, whereas the rest are based on the Paris potential. For this observable we also note that σ_R based on the AV18 interaction, within the ABL approach, falls outside the range defined by the three folding approaches using the Paris interaction. Additionally,

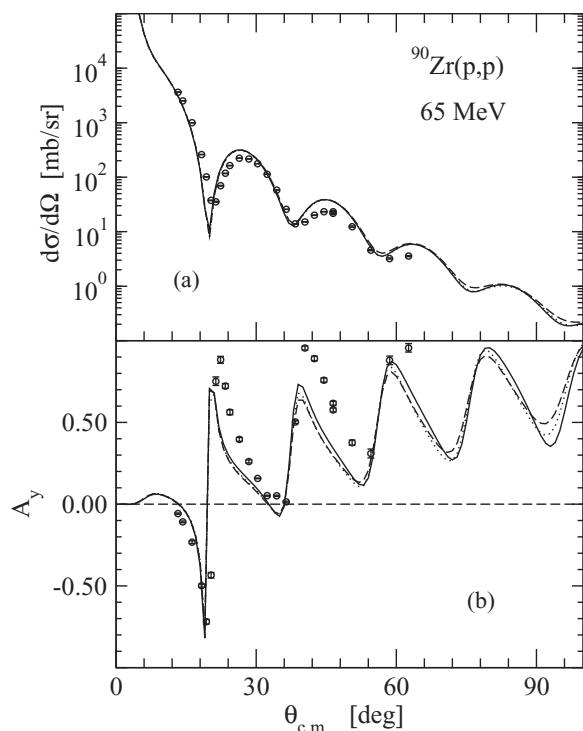


FIG. 6. The same as Fig. 5 but at 65 MeV. The data are from Ref. [31].

the differences among these three schemes appear more pronounced in the case of ^{16}O , becoming marginal for ^{90}Zr .

From the results we have reported thus far, some lack of consistency in accounting for the data becomes evident. We must stress, however, that our main goal here has been that of providing a comprehensive account of the seven-dimensional folding integral, contrasting its predictions with those based on simplified expressions. Thus, we have chosen at this point not to explore ways to improve the description of the data.

C. Sensitivity of the pair total momentum

A comparison of the results reported here with those based on folding models at similar energies [8,35], using local density-dependent effective interactions, poses the question of what may be the causes for differences in the predictions. In this respect it is important to keep in mind that in the construction of local effective interactions for NA scattering, specific prescriptions for the total momentum and starting energies of the interacting pair are introduced. Indeed, in Refs. [8,9] the density-dependent effective interactions are localized by taking the on-shell momentum of the projectile (\vec{k}) from

$$E \equiv e(\vec{k}) = \frac{\vec{k}^2}{2m} + U_{k_F}(\vec{k}), \quad (15)$$

where E is the beam energy and $U_{k_F}(k)$ is the self-consistent field in the Brueckner-Bethe-Goldstone equation at Fermi momentum k_F . In Ref. [35] instead, the total momentum is given by an average which depends on the density and the momentum of the beam, where the struck-nucleon momentum

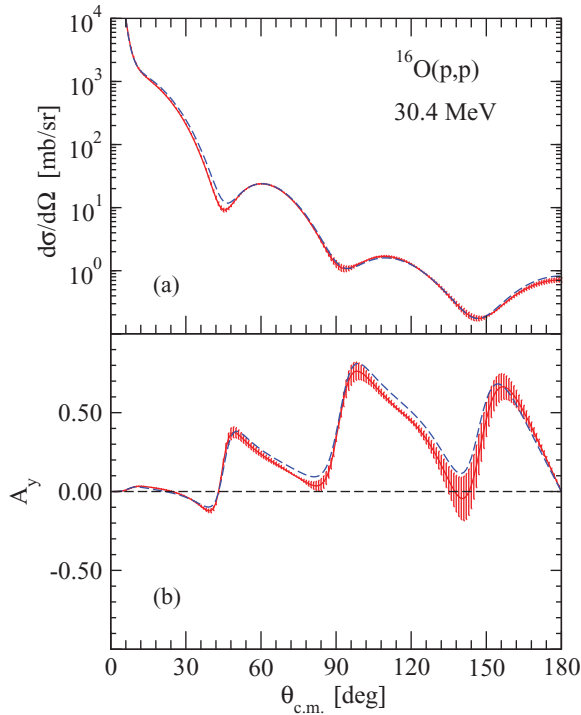


FIG. 7. (Color online) Calculated $d\sigma/d\Omega$ (a) and A_y (b) as functions of $\theta_{c.m.}$ for $^{16}\text{O}(p,p)$ at 30.4 MeV. The solid curves are based on the Paris potential, representing the average from unabridged, δg -folding, and ABL-folding; the bars extend from the lowest to the highest values. Dashed curves represent ABL results using the AV18 potential.

is evaluated at the average value $k^* = 0.8536k_F$. These relationships effectively boost the momentum of the projectile, a feature not emulated in the calculations presented here. Not only that, but the localization itself is designed to reproduce only part of the g matrix: the forward on-shell amplitude in the case of Refs. [8,9] and half-off-shell amplitude in the case of Ref. [35]. In contrast to both approaches, in this work no localization to the g matrix is pursued, with the total momentum of the interacting pair kept at the Fermi-averaged momentum $\langle \mathbf{k} + \mathbf{p} \rangle$, while $k^2 = 2mE$ and $|\mathbf{p}| \leq k_F$. The starting energy is $\omega = E + \langle e(p) \rangle$. The dependence on the relative momenta is treated exactly as dictated by the kinematics of the collisions.

For the purpose of illustrating the level of sensitivity to a chosen prescription for the total momentum, we have performed calculations of optical potentials in the ABL framework by evaluating the g matrix at a total momentum given by $\langle \mathbf{k} + \mathbf{p} \rangle$, where \mathbf{k} is obtained from Eq. (15). For a given energy E , each density (or Fermi momentum) defines its corresponding \mathbf{k} . In Fig. 9 we compare ABL-folding calculations using the standard (solid curves) and boosted (dashed curves) prescriptions for the total momentum, in the case of proton scattering at 30 MeV. The data are the same as in Figs. 1 and 4. As observed, a substantial improvement in the description of the zirconium data is observed, with the differential cross section in phase with the measurements. In the case of the oxygen data, however, the improvement is

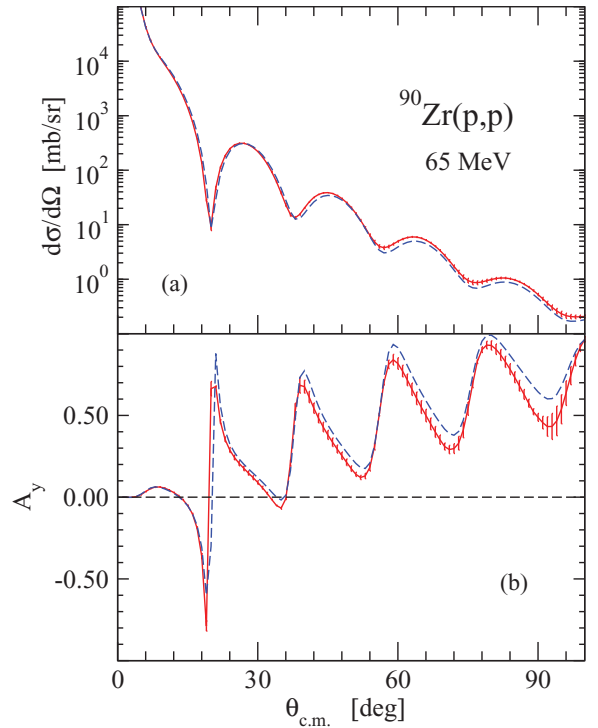


FIG. 8. (Color online) The same as Fig. 7 but for $^{90}\text{Zr}(p,p)$ at 65 MeV.

quite moderate. A broader exploration, including other targets and higher energies, shows that the improvement is not robust enough to be considered confidently. Additionally, we find that the scattering observables become quite sensitive to the choice of the starting energy at which one evaluates the g matrix, particularly at low energies. In any case, the illustration shown here suggests that there is room for improvement in the description of the data. The issue then is to identify a prescription, supported by the theory, which may lead to an eventual improvement. Such a study is left for future investigation.

An additional element which needs to be included in these comparisons is the way the Brueckner-Bethe-Goldstone integral equation is solved, particularly with respect to the treatment of the angular structure of the energy denominator. In Ref. [35] the self-consistent fields are given a quadratic

TABLE I. Calculated reaction cross sections for proton elastic scattering following the unabridged, δg , and ABL folding models.

Target	energy (MeV)	σ_R			
		Unabridged (b)	δg (b)	ABL (b)	ABL ^a (b)
^{16}O	30.4	0.656	0.643	0.650	0.619
	49.48	0.527	0.510	0.515	0.491
	65	0.461	0.444	0.448	0.427
^{90}Zr	30	1.40	1.40	1.39	1.38
	40	1.40	1.39	1.39	1.36
	65	1.29	1.26	1.28	1.24

^aBased on AV18.

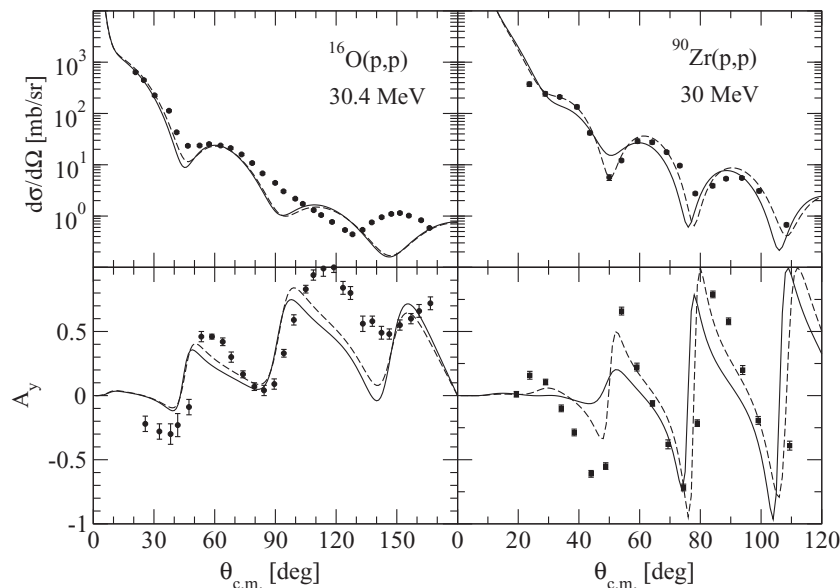


FIG. 9. Measured [29,32] and calculated differential cross section (upper frames) and analyzing power (lower frames), as functions of the center-of-mass scattering angle, for $^{16}\text{O}(p,p)$ (30.4 MeV) and $^{90}\text{Zr}(p,p)$ (30 MeV) scattering. The solid and dashed curves represent ABL-folding results with standard and boosted center-of-mass momentum, respectively.

representation, leading to the so-called effective-mass approximation. In the work presented here we use the angular average of the two-particle fields. However, as reported in Ref. [36], a more refined treatment to the angular structure of the energy denominator shows that NA scattering observables are sensitive to the way the g matrix and corresponding self-consistent fields are calculated. These observations need to be taken into account for a broad and rigorous assessment of the theory.

IV. SUMMARY AND CONCLUSIONS

We have presented the first realization of the seven-dimensional *in-medium* folding optical model, where the off-shell structure of the effective interaction, as well as the exact kinematics of the colliding nucleons, is retained. This unabridged potential is based on the general momentum- and coordinate-space structure of any two-body interaction, where the introduction of a mean coordinate leads naturally to a local density approximation for the reduced interaction. The use of the asymptotic separation introduced in Ref. [12] has been pivotal for the actual evaluation of the potential, confining the intrinsic medium contributions to regions where the gradient of the density is more pronounced. The density-dependent effective interaction is modeled by means of infinite nuclear matter g -matrix solutions of the Brueckner-Bethe-Goldstone equation. We have based our study on the Paris NN bare interaction.

Applications were made for proton elastic scattering from ^{16}O and ^{90}Zr at energies between 30 and 65 MeV. Scattering observables based on unabridged optical model calculations were compared to those from two alternative approximations. One of them is the δg -folding approach, where the recoil of the struck nucleon is treated as if the total momentum of the interacting pair was conserved. The other approach was the ABL-folding where, in addition to the above consideration, the mixed density is treated within the Slater approximation. Their corresponding CPU times needed to

evaluate the potentials appear in the ratio 500:20:1. Despite these significant ratios in computing time, only moderate differences are observed among the three calculating schemes, being more pronounced in the case of $^{16}\text{O}(p,p)$ scattering at 30 MeV. In this respect, we conclude that the δg -folding and ABL-folding approaches constitute reliable representations of the unabridged optical model, at least above 30 MeV. The advantage of the δg -folding lies in its ability to treat explicitly the full (off-shell) mixed density, contrasting with the ABL approach, which needs only the diagonal mixed density (or radial density).

In order to estimate the error implied by approximate treatments to the optical potential, we evaluated optical potentials in the ABL approach using the AV18 NN interaction. We found that, for the two NN potentials considered, the uncertainties due to these descriptions are larger than the ones attainable to the treatment of the kinematics and/or representation of the mixed density. In this regard, the δg - and ABL-folding models can be considered reliable representations of the unabridged model. Certainly this statement depends on the expected accuracy, but considering the fact that in many cases the discrepancies between data and theory may be significant, these two models convey enough simplicity and versatility to make them useful for expedited studies. In any case, with this study we have demonstrated that the evaluation of the unabridged optical potential is feasible with current computing capabilities.

ACKNOWLEDGMENTS

H.F.A. acknowledges funding from and the generous hospitality of colleagues at CEA/DAM/DIF, Bruyères-le-Châtel, France, during his sabbatical leave where part of this research took place. The authors are thankful to the CCRT (Centre de Calcul, Recherche et Technologie) for use of the multiprocessor facilities at CEA. This work has been funded in part by FONDECYT under Grant No. 1080471 and by VID-UCH under Grant No. ENL1106.

- [1] K. M. Watson, *Phys. Rev.* **89**, 575 (1953).
- [2] H. Feshbach, *Ann. Phys. (NY)* **5**, 357 (1958); **19**, 287 (1962).
- [3] A. K. Kerman, H. McManus, and R. M. Thaler, *Ann. Phys. (NY)* **8**, 551 (1959).
- [4] A. L. Fetter and K. M. Watson, in *Advances in Theoretical Physics*, Vol. 1, edited by K. A. Brueckner (Academic, New York, 1965).
- [5] F. Villars, in *Fundamentals in Nuclear Theory*, edited by A. de Shalit and C. Villi (International Atomic Energy Agency, Vienna, 1967).
- [6] L. Ray, G. W. Hoffmann, and W. R. Coker, *Phys. Rep.* **212**, 223 (1992).
- [7] K. Amos, P. J. Dortmans, H. V. von Geramb, S. Karataglidis, and J. Raynal, in *Advances in Nuclear Physics*, Vol. 25, edited by J. W. Negele and E. Vogt (Kluwer Academic/Plenum Publishers, New York, 2000), p. 275.
- [8] F. A. Brieva and J. R. Rook, *Nucl. Phys. A* **291**, 317 (1977); **307**, 493 (1978).
- [9] H. V. von Geramb, in *The Interaction Between Medium Energy Nucleons in Nuclei*, edited by H. O. Meyer (American Institute of Physics, New York, 1983).
- [10] H. F. Arellano, F. A. Brieva, and W. G. Love, *Phys. Rev. C* **52**, 301 (1995).
- [11] F. J. Aguayo and H. F. Arellano, *Phys. Rev. C* **78**, 014608 (2008).
- [12] H. F. Arellano and E. Bauge, *Phys. Rev. C* **76**, 014613 (2007).
- [13] See, e.g., [<http://www.eurisol.org/>].
- [14] See, e.g., [<http://isolde.web.cern.ch/isolde/>].
- [15] See, e.g., [<http://www.ganil-spiral2.eu/>].
- [16] See, e.g., [<http://www.rarf.riken.go.jp/Eng/>].
- [17] See, e.g., [<http://www.nsl.msu.edu/>].
- [18] See, e.g., [<http://isolmyrrha.sckcen.be/en/>].
- [19] H. F. Arellano, F. A. Brieva, and W. G. Love, *Phys. Rev. Lett.* **63**, 605 (1989).
- [20] H. F. Arellano, F. A. Brieva, and W. G. Love, *Phys. Rev. C* **41**, 2188 (1990).
- [21] Ch. Elster, T. Cheon, E. F. Redish, and P. C. Tandy, *Phys. Rev. C* **41**, 814 (1990).
- [22] R. Crespo, R. C. Johnson, and J. A. Tostevin, *Phys. Rev. C* **41**, 2257 (1990).
- [23] X. Campi and A. Bouyssi, *Phys. Lett. B* **73**, 263 (1978).
- [24] J. W. Negele, *Phys. Rev. C* **1**, 1260 (1970).
- [25] M. Lacombe, B. Loiseau, and J. M. Richard, and R. Vinh Mau, J. Côté, P. Pirés, and R. de Tourreil, *Phys. Rev. C* **21**, 861 (1980).
- [26] H. F. Arellano and H. V. von Geramb, *Phys. Rev. C* **66**, 024602 (2002).
- [27] H. F. Arellano, F. A. Brieva, and W. G. Love, *Phys. Rev. C* **50**, 2480 (1994).
- [28] H. F. Arellano and W. G. Love, *Phys. Rev. C* **76**, 014616 (2007).
- [29] P. D. Greaves, V. Hnizdo, J. Lowe, and O. Karban, *Nucl. Phys. A* **179**, 1 (1972).
- [30] J. A. Fannon, E. J. Burge, D. A. Smith, and N. K. Ganguly, *Nucl. Phys. A* **97**, 263 (1967).
- [31] H. Sakaguchi, M. Nakamura, K. Hatanaka, A. Goto, T. Noro, F. Ohtani, H. Sakamoto, H. Ogawa, and S. Kobayashi, *Phys. Rev. C* **26**, 944 (1982).
- [32] R. de Swiniarski, D.-L. Pham, and G. Bagieu, *Can. J. Phys.* **55**, 43 (1977).
- [33] L. N. Blumberg, E. E. Gross, A. van der Woude, A. Zucker, and R. H. Bassel, *Phys. Rev.* **147**, 812 (1966).
- [34] R. B. Wiringa, V. G. J. Stoks, and R. Schiavilla, *Phys. Rev. C* **51**, 38 (1995).
- [35] P. J. Dortmans and K. Amos, *Phys. Rev. C* **49**, 1309 (1994).
- [36] H. F. Arellano and J.-P. Delaroche, *Phys. Rev. C* **83**, 044306 (2011).